The Mechanism of Rhodium Catalyzed Allylic C–H Amination

Robert J. Harris,[†] Jiyong Park[‡,§], Taylor A. F. Nelson,[†] Nafees Iqbal,[‡,§] Daniel C. Salgueiro,[†] John Bacsa,[†] Cora E. MacBeth,[†] Mu-Hyun Baik*[,§,‡] and Simon B. Blakey*[,†]

[†]Department of Chemistry, Emory University, Atlanta, GA, 30322, U.S.A.

[‡]Department of Chemistry, Korea Advanced Institute of Science and Technology (KAIST), Daejeon 34141, Republic of Korea

[§]Center for Catalytic Hydrocarbon Functionalizations, Institute for Basic Science (IBS), Daejeon 34141, Republic of Korea

ABSTRACT

The mechanism of catalytic allylic C–H amination reactions promoted by Cp*Rh complexes is reported. Reaction kinetics experiments, stoichiometric studies, and DFT calculations demonstrate that allylic C–H activation to generate a Cp*Rh(π-allyl) complex is viable under mild reaction conditions. The role of external oxidant in the catalytic cycle is elucidated. Quantum mechanical calculations, stoichiometric reactions, and cyclic voltammetry experiments support an oxidatively induced reductive elimination process of the allyl fragment with an acetate ligand. Lastly, evidences supporting the amination of an allylic acetate intermediate is presented. Both nucleophilic substitution catalyzed by Ag^+ that behaves as a Lewis acid catalyst and an inner-sphere amination catalyzed by Cp*Rh are shown to be viable for the last step of the allylic amination reaction.

Keywords: Density Functional Theory, C–H amination, Rhodium, Allylic functionalization, Mechanism

INTRODUCTION

Transition-metal-mediated direct activation of C(sp^3)–H bonds to install C–X (X = C, N, and O) functionalities has become an indispensable method in modern synthetic strategy. Precisely controlling the regio- and diastereo-selectivities in these reactions is a key challenge that has been achieved using directing groups[1] or by taking advantage of the inherent reactivities of the C–H bonds.[2] Direct and efficient synthetic protocols that afford desired selectivities continue to be actively sought after. In 2004, White and co-workers reported the catalytic allylic C–H acetoxylation of terminal olefins in complex settings catalyzed by palladium.[3] In a series of reports that followed, Pd(π-allyl) intermediates were intercepted with a variety of stabilized carbon, nitrogen, and oxygen nucleophiles (Scheme 1a).[4] Cossy and co-workers subsequently reported the use of Cp*Rh to catalyze the intramolecular cyclization of aminoalkenes by allylic C–H functionalization, as illustrated in Scheme 1b.[5] More recently our group disclosed the intermolecular allylic C–H amination of internal aryl and alkyl alkenes with primary and secondary amines bearing only one electron withdrawing group (Scheme 1c).[6]

Scheme 1. Transition metal catalyzed allylic C–H amination with nucleophilic amines

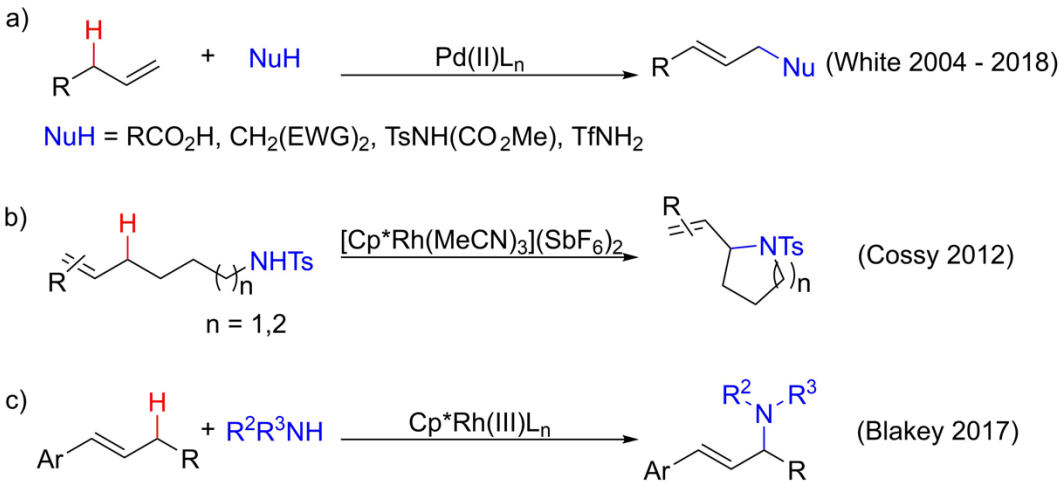

The development of catalytic methods for C(sp^3)–H functionalization has exceeded our mechanistic understanding of these transformations. In the case of rhodium catalyzed allylic C–H functionalization, Cossy suggested that a plausible mechanism would involve an allylic C–H insertion to generate a Rh(π-allyl) complex followed by *N*-metallation and reductive elimination from a Rh(III) intermediate to generate the allylic amine and a Rh(I) species that would be reoxidized to Rh(III) to complete the catalytic cycle. This mechanism is in accord with reports on the rhodium catalyzed allylic substitution with phosphine and phosphite supporting ligands.[7] Similar catalytic reactions involving Rh(III/I) have also been proposed for C(sp^2)–H bond activations that utilize cyclopentadienyl supporting ligands.[8] However, we note that higher oxidation states of rhodium have also been proposed in Cp*Rh catalyzed C(sp^2)–H activation.[9]

Providing additional complexity to the mechanistic picture, the synthesis and reactivity of several group IX π-allyl complexes similar to those invoked by Cossy and our group in the Cp*Rh catalyzed allylic C–H amination have been reported. Bergman isolated and characterized the Cp*Rh(π-allyl) complex **I** (Figure 1a)[10] and Stryker

subsequently determined the structures of the *exo* and *endo* isomers of IrCp*(π-allyl) complex **II** (Figure 1b).[10b] In each case, the *exo*-isomers of the π-allyl complexes react with hard nucleophiles at the central carbon to generate metallocyclobutane products. Additionally, Tanaka reported the isolation and characterization of the Rh(III)Cp^E(π–allyl) complex **III** bearing a pendent tosyl amine nucleophile (Figure 1c).[10c] When complex **III** was treated with $AgSbF_6$ to abstract the chloride and generate a vacant coordination site for *N*–metallation, the expected cyclization product was not observed. When complex **III** was treated with both $AgSbF_6$ and $Cu(OAc)_2$, the expected amination product was observed in 51% yield. The authors did not postulate specific roles of $Cu(OAc)_2$ in this transformation. However, Jones and coworkers have reported the use of a copper salt as an oxidant to induce reductive elimination of a C(sp2)–N(sp2) bond from a Cp^*Rh^{III}complex.[9b] In 2017, Chang and Baik reported a detailed mechanistic study of a C–H arylation reaction catalyzed by Cp*Ir, in which a strong oxidant facilitates the C–H arylation by oxidizing the metalated π–allyl complex via an oxidatively induced reductive elimination (Figure 1d).[11]

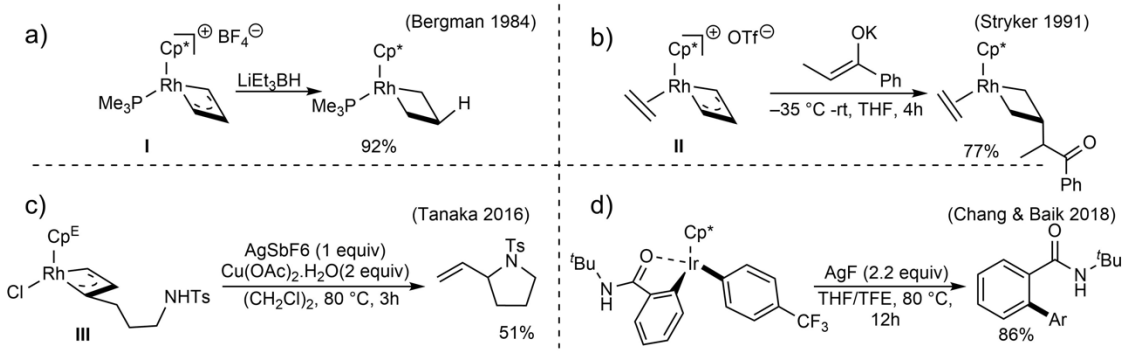

Figure 1. Previously reported reactions of group IX π-allyl complexes

The reactivity of π-allyl complexes (**I**-**III**) is largely inconsistent with the previously proposed Rh(III/I) mechanism for Cp*Rh catalyzed allylic C–H amination. Herein, we describe a detailed study combining experimental observations including kinetic analysis, isolation and characterizations of reactivities of putative intermediates, and cyclic voltammetry measurements, that are corroborated with quantum mechanical calculations, to elucidate the mechanism of the Rh-catalyzed $C(sp^3)$–H activations that afford allylic amination products.

RESULTS AND DISCUSSION

Kinetic analysis: To obtain experimental data to facilitate a deeper understanding of the mechanism for the rhodium catalyzed allylic C–H amination, we targeted 1,3-diphenylpropene **1** as a simple model substrate, in which complications caused by regioselectivity are not present (eq 1). We note that our initial attempt to monitor the reaction progress using *p*-toluenesulfonamide as a nucleophile was complicated due to its insolubility, leading us to choose benzyl carbamate as the nucleophile.

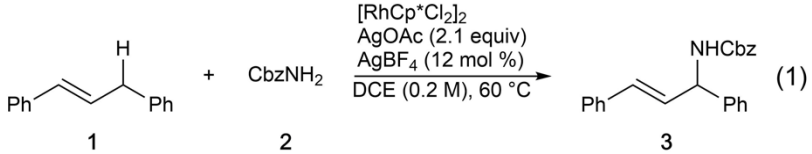

Analysis of initial rates of reactions of diphenylpropene **1** with benzyl carbamate **2** catalyzed by $[Cp^*RhCl_2]_2/AgBF_4$ showed that allylic amine production was linearly dependent on the concentrations of the Rh,

alkene, and carbamate with slopes of $k_1 = 2.4 \pm 0.4 \times 10^{-4}$ s^{-1}, $k_2 = 1.5 \pm 0.1 \times 10^{-5}$ s^{-1} and $k_3 = -5.2 \pm 0.6 \times 10^{-5}$ s^{-1} respectively (Figures S2-S4). These data indicate the reaction is first-order in rhodium and alkene concentrations. Also an inverse rate constant for the carbamate concentration was observed, that is consistent with the carbamate nucleophile binding to the rhodium catalyst in an off cycle equilibrium (Scheme S1).

Deuterium exchange experiments provide insight into the rate determining step (RDS). A 1:1 mixture of **1** and **1**-d_2 (0.2 M) in DCE was treated with benzyl carbamate **2** (0.49 M), $[Cp^*RhCl_2]_2$ ([Rh] = 12 mM), $AgBF_4$ (26 mM), and AgOAc (2.1 equiv). The reaction was stopped after 2 hours (~10% conversion), and allylic amine **3** was isolated in 5% yield (Figure 2). Analysis of the ^{1}H NMR of **3** established a 14% deuterium incorporation at both C1 and C3, which is consistent with a primary KIE of $k_H/k_D = 2.5$. In our original disclosure of the rhodium catalyzed allylic C–H amination, we showed that C–H cleavage was irreversible.[6] Taken together, these observations along with the first order dependence of rate on **1**, establish that C–H cleavage is rate-determining.[11]

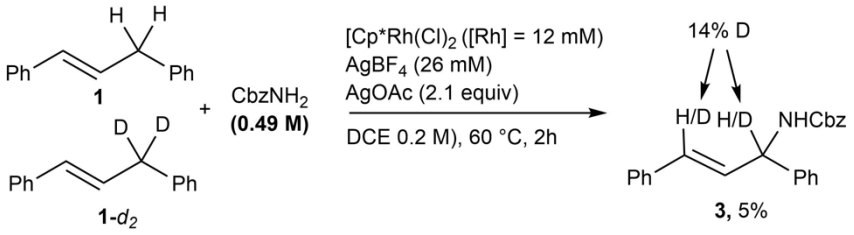

Figure 2. Amination of a 1:1 mixture of **1** and **1**-d_2 with benzyl carbamate catalyzed by $[Cp^*RhCl_2]_2$

Synthesis, Characterization, and Reactivity of rhodium π-allyl complexes

The kinetic data presented above are consistent with the notion that C–H activation step is rate limiting, and consequently overall reaction kinetics cannot be used to probe the mechanism of C–N bond formation or catalyst regeneration. In order to gain insight into this sequence in the catalytic cycle, we synthesized plausible putative intermediates in the catalytic cycle and examined their reactivities. Analogous to Tanaka's synthesis of Cp^ERh(π-allyl) complex **III**, we attempted to synthesize a Rh(π-allyl) complex with a Cp* supporting ligand. Initial attempts to make to make a Cp*Rh(π-allyl) complex starting from $[Cp^*RhCl_2]_2$ in the presence of $AgSbF_6$ were unsuccessful and led to a complex mixture of products. However, stirring $[Cp^*Rh(NCMe)_3](SbF_6)_2$ with cesium acetate (1.5 equiv) and 4-phenyl-1-butene (2 equiv) in CH_2Cl_2 at room temperature for 16 h followed by the addition of tetraethylammonium chloride, lead to the isolation of a mixture of Rh(π-allyl) complexes **IV** and **V** in 53% yield (9:1 ratio, Figure 3a). By using DCE as a solvent and heating the reaction to 80 °C we were able to isolate complex **V** exclusively as the thermodynamic product in 61% yield (Figure 3b).

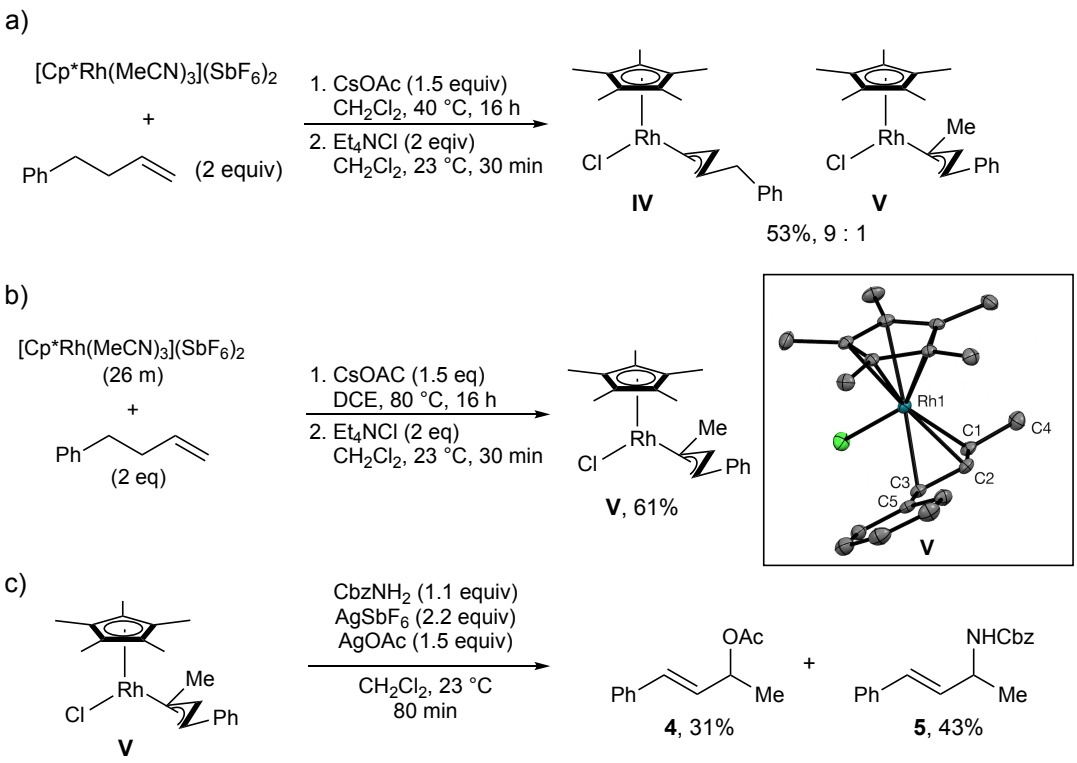

Figure 3. Synthesis and structure of Cp*Rh(π-allyl)Cl complex. ORTEP diagram of **V** depicted with ellipsoids shown at the 50% probability level and hydrogen atoms omitted for clarity

Complex **V** was fully characterized by ^{1}H and ^{13}C NMR spectroscopy and single crystal X-ray diffraction. The ^{1}H NMR spectrum of **V** displayed a characteristic triplet of doublets at δ = 4.55 ppm with coupling constants J_{HH} = 10.7 Hz and J_{RhH} = 2.0 Hz corresponding to the proton attached to the central carbon of the π-allyl ligand. Vapor diffusion of pentane into a concentrated ether solution of **V** at 25 °C provided crystals suitable for X-ray analysis (Figure 3b, inset). The allyl ligand of complex **V** adopts a near planar geometry with dihedral angles C1–C2–C3–C5 = 173.8° and C4–C1–C2–C3 = 178.6°. The Rh–C1 and Rh–C3 bond distances are approximately equal with bond lengths of 2.203(2) and 2.219(2) Å respectively while the Rh–C2 bond length is significantly shorter with a bond length of 2.133(2) Å.

With complex **V** in hand, we began to investigate Cp*Rh(π-allyl) complexes' reactivity toward nucleophiles. In an initial experiment, complex **V** was treated with a single equivalent of benzyl carbamate **2** in CH_2Cl_2 at 23 °C. Unsurprisingly, even after 48 h, complex **V** remained unreacted. However, when complex **V** was treated with benzylcarbamate (**2**, 1.1 equiv) in the presence of $AgSbF_6$(2.2 equiv, as a halide abstractor) and AgOAc (1.5 equiv) in CH_2Cl_2at 23 °C to mimic the reaction conditions that yielded aminated products, allylic acetate **4** and the expected allylic amine **5** were generated in 31% and 43% yield respectively (Figure 3c). This result suggests that while **V** is likely not a catalytically relevant species, the cationic complex generated from abstracting a chloride from **V** could be. Also the result indicate that silver additives are essential for the activation of the Rh(π-allyl) complex **V**. Lastly, the significant quantities of allylic acetate **4** observed in the reaction lead us to consider the possibility that the amination reaction might proceed through an allylic acetate intermediate.

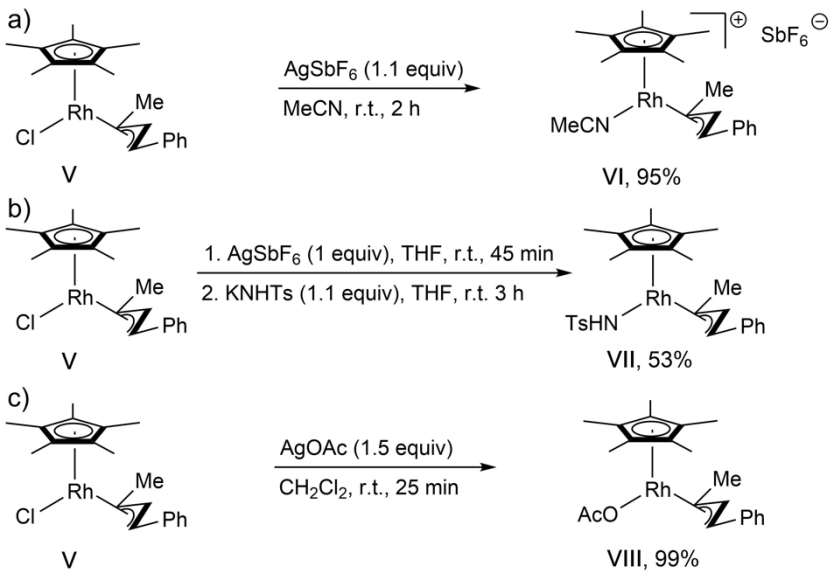

Figure 4. Synthesis of Cp*Rh(III)(π-allyl) complexes bearing acetonitrile, tosylamine and acetate ligands

To further probe these possibilities we synthesized the cationic Cp*Rh(π-allyl)(MeCN)(SbF_6) complex **VI** (Figure 4a), the Cp*Rh(π-allyl)(NHTs) complex **VII** (Figure 4b) and the Cp*Rh(π-allyl)(OAc) complex **VIII** (Figure 4c). Complexes **VI**, **VII** and **VIII** were characterized by ^{1}H and ^{13}C NMR spectroscopy and **VII** and **VIII** were further characterized by single crystal X-ray diffractions (Figures S5 and S6). The isolation of complexes **VII** and **VIII** unambiguously rules out the possibility that allylic C-N or C-O bond formation by reductive elimination from these Rh(III) species is possible under the catalytic conditions (Figures S5 and S6). Furthermore, the fact that no allylic amine or allylic acetate product was observed during the synthesis of complexes suggests that outer-sphere nucleophilic attack of these nucleophiles on cationic Rh(III)(π-allyl) complexes is also not a plausible explanation for product formation in the catalytic reaction.

This conclusion is further supported by the observation that when cationic complex **VI** was reacted with benzylcarbamate at 40°C for 14h that did not yield allylic amine. Instead, Cp*Rh(π-allyl)Cl complex **V** was recovered in 92% yield after a chloride quench (Figure 5a). To investigate the potential for an oxidatively induced reductive elimination mechanism to be operating, we exposed both Cp*Rh(π-allyl)(NHTs) complex **VII** and Cp*Rh(π-allyl)(OAc) complex **VIII** to two equivalents $AgSbF_6$. In the reaction of Cp*Rh(π-allyl)(NHTs) complex **VII**, two equivalents of benzensulfonamide were included that allows us to probe both an oxidatively induced inner-sphere reductive elimination, and an oxidatively induced outer-sphere nucleophilic attack. In this reaction, only 10% combined yield of allylic amine products (**6** and **7)** was observed. No rhodium(π-allyl) complexes could be recovered (Figure 5b). In contrast, when the Cp*Rh(π-allyl)(OAc) complex **VIII** was oxidized with two equivalents $AgSbF_6$, clean conversion to the allylic acetate product **4** was observed (Figure 5c). These observations suggest that the catalytic allylic amination reactions proceed through an allylic acetate intermediate, obtained by an oxidatively induced reductive elimination mechanism.

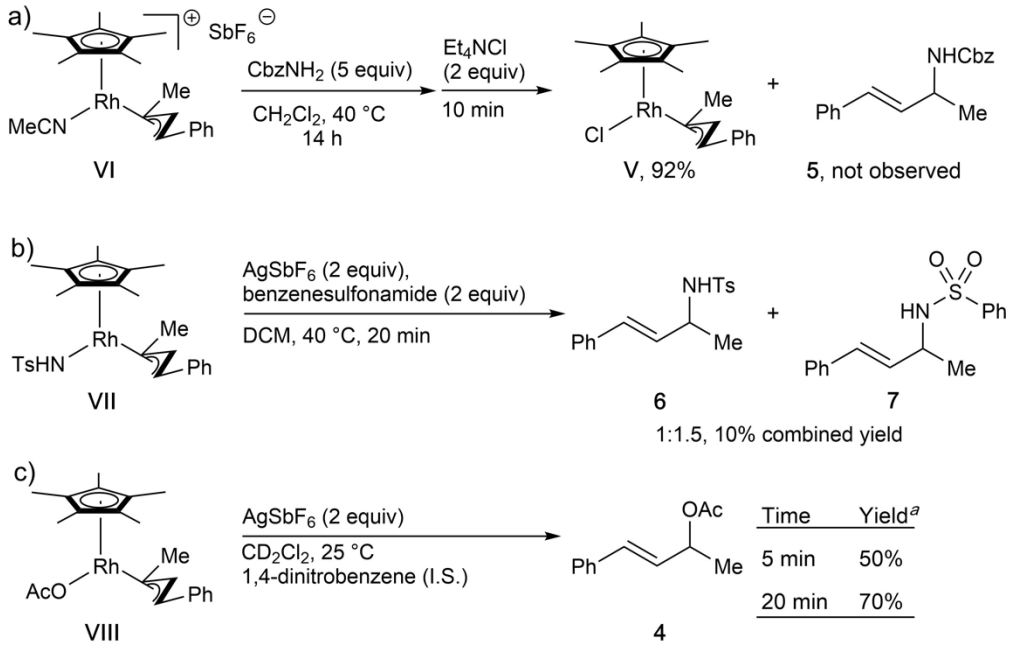

Figure 5. Reactivity of Cp*Rh(III)(π-allyl) complexes demonstrating the feasibility of oxidatively induced reductive elimination of an allyl acetate. [a]Yields were determined by ^{1}H NMR analysis of the reaction mixture using 1,4-dinitrobenzene as an internal standard.

To complete our experimental investigation, we demonstrated that allylic acetate **4** is readily converted to the allylic amine **3** in the presence of the Lewis acid components present in the catalytic reactions (Table 1). Both cationic Ag(I) and cationic Rh(III) are able to promote this reaction. In the absence of either silver cation or Cp*Rh, the allylic acetate remained unchanged. These data provide a plausible hypothesis of the pathway toward the completion of the allylic amination catalytic cycle.

Table 1. Reactivity of allylic acetate **4** benzyl carbamate **2** in the presence of Ag(I) or Rh(III) as a catalyst.

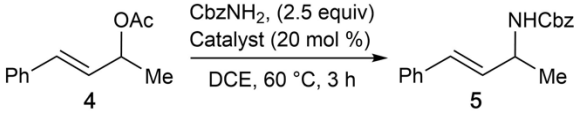

entry	Catalyst	Yield
1	$AgSbF_6$	91%
2	$AgBF_4$	76%
3	$[Cp^*RhCl_2]_2/AgSbF_6$[a]	73%
4	$[Cp^*Rh(NCMe)_3](SbF_6)_2$	84%
5	none	0%[b]

[a]$[Cp^*RhCl_2]_2$ (25 mM) and $AgSbF_6$ (40 mM) were stirred in DCM with benzyl carbamate (**2**) at 60 °C for 30 min before allylic acetate **6** was added to be sure that there was no Ag^+ in solution. [b]Allylic amine was not observed by ^{1}H NMR.

Computational Investigation of the key steps in the catalytic cycle

Density functional theory (DFT) calculations were carried out to construct a catalytic mechanism incorporating the experimental observations mentioned above. Using 1,3-diphenylpropene **1** as the substrate, we compared the activation barriers of the reductive elimination from the three relevant oxidation states Rh(III), Rh(IV) and Rh(V), as illustrated in Figure 6. The reductive elimination initiated from the Rh(III) intermediate to give Rh(I) is not viable, as the computed activation barrier of 38.4 kcal/mol corresponds to an Eyring rate of 0.6×10^{-10} mol/day at 298 K (Figure 6a). As expected, the oxidation of the metal center to Rh(IV) lowers the activation barrier notably by more than 21 kcal/mol to 17.6 kcal/mol (Figure 6b), which suggests an acceleration of the reaction by more than 10^{10} fold compared to the Rh(III) intermediate. Our calculations suggest that a second oxidation to access the Rh(V) center does not enhance the reaction rate further, as the calculated barrier increases to 19.5 kcal/mol (Figure 6c).

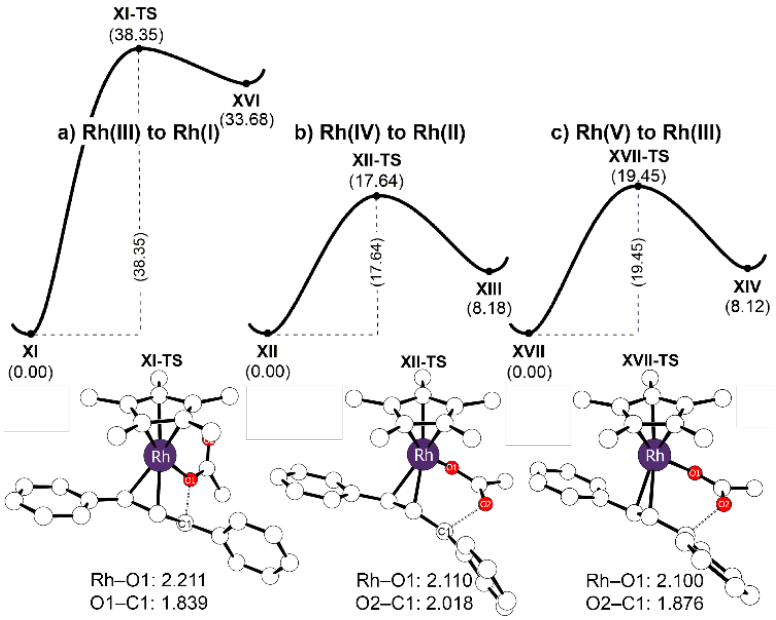

Figure 6. Calculated energy profiles for reductive elimination from the a) Rh(III)–, b) Rh(IV)–, and c) Rh(V)–π-allyl intermediates, leading to the Rh(I), Rh(II), and Rh(III) products, respectively. The detailed molecular structure of each TS is shown as well. The unit of energy is kcal/mol and of bond length is Å.

A closer inspection of the transition structures reveals that the two oxygen atoms of the acetate introduce a slight variation in the transition states. During the reductive elimination from the Rh(III)-center, the O–C bond is formed by the acetate-oxygen that is directly bound to the metal, as illustrated in Figure 6a. The Rh–O bond elongates from 2.121 to 2.211 Å as the transition state **XI-TS** is traversed with the C–O distance being 1.839 Å. This bond forming event is best conceptualized by considering that the allylic fragment formally donates two electrons to the Rh-center to accomplish the reductive part of the reductive elimination step. Consequently, it becomes a positively polarized electrophile that can engage the acetate and form the C–O bond. Of course, these two processes are concerted in reality, but it is instructive to visualize them separately. When the metal is oxidized

to Rh(IV) or Rh(V), it is the distal oxygen of the acetate that attacks the carbon and the Rh–O bond is mostly maintained with the Rh–O bond lengths being 2.110 (**XII-TS**) and 2.100 Å (**XVII-TS**), respectively, as illustrated in Figures 6b and 6c. Thus, whereas the Rh(III) center carries out a classical reductive elimination, the other higher valent metal centers prefer to reductively couple the acetate with the allyl functionality without eliminating the acetate. This subtle change in mechanism is easy to understand considering that the Rh–O bond becomes much stronger in Rh(IV) and Rh(V) compared to Rh(III). As the acetate acts as a nucleophile in this step, the higher oxidation state at the metal decreases its nucleophilicity and results in a higher barrier in the Rh(V)-complex. Thus, Rh(IV) constitutes an ideal compromise between the two governing forces, namely the ability of the metal center to oxidize the allyl fragment and the nucleophilicity of the acetate.

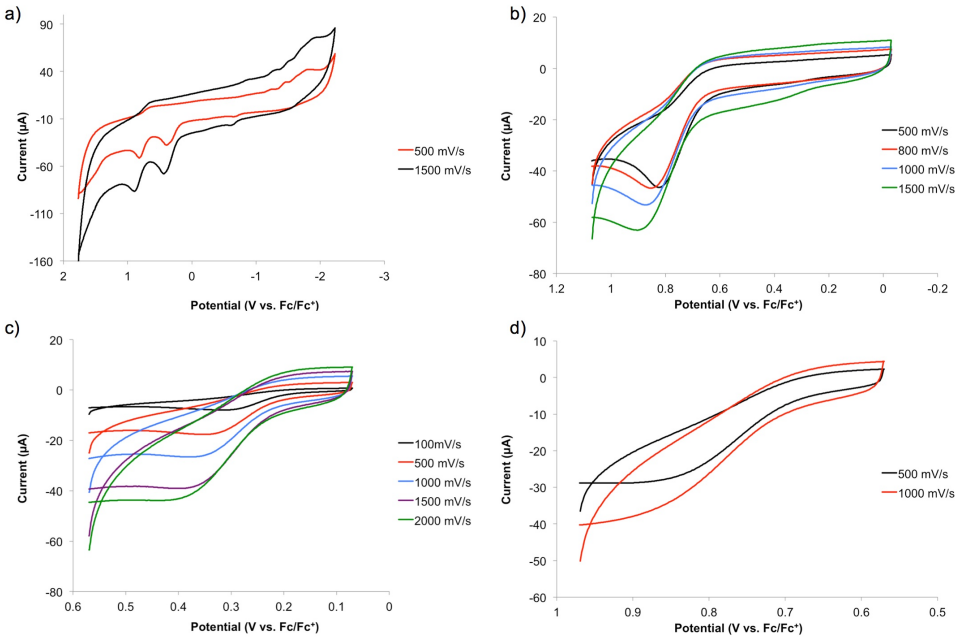

Figure 7. Cyclic voltammograms of rhodium acetate complex **VIII**. Voltammograms recorded in CH_2Cl_2 with 0.1 M $TBAPF_6$ as the supporting electrolyte.

To test the proposed catalytic mechanism, cyclic voltammetry experiments were carried out. Complex **VIII** showed two irreversible oxidation waves, suggesting that both Rh(IV) and Rh(V) are accessible on an electrochemical time scale (Figures 7a and 7b). As is expected for an electrochemical step that is coupled with a chemical event, the peak position of both steps are scan rate dependent (Figures 7c and 7d). The first oxidation occurs at E_p = ~0.42 V versus Fc/Fc^+ which we assign to the Rh(III)/(IV) couple, and the second event occurs at E_p = ~0.85 V that is attributed to the Rh(IV)/(V) couple. Importantly, even at fast scan rates of 2,000 mV/s the Rh(III)/(IV) redox event is irreversible suggesting that reductive elimination from Rh(IV) is fast (Figure 7c). Given that the redox potential of Ag^+ in CH_2Cl_2 is 0.65 V, it is unlikely that the Rh(V) complex can be accessed via chemical oxidation. Taken together, these data support a catalytic cycle that consists of the sequence Rh(III) → Rh(IV) → Rh(II) → Rh(III).

Scheme 2 summarizes the proposed mechanism of the Rh catalyzed allylic acetylation and the corresponding reaction energy profile is shown in Figure 8. The catalytic cycle begins with the coordination of the acetate and the olefin substrates **1** to the Cp*Rh fragment to form the initial reactant complex **IX**, which undergoes a concerted metalation deprotonation (CMD) traversing the transition **VI-TS** to activate the allylic C–H bond. The computed activation energy for this step is 26.7 kcal/mol, which is in good agreement with the experimental observation that a mildly elevated temperature is required to prepare the acetylated intermediate **XIII** (*vide supra*). Ligand exchange affords the Cp*Rh(III)(π-allyl)OAc complex **XI**. As discussed above, reductive elimination from this intermediate is associated with a very high barrier (Figure 6a). To push the reaction forward, one electron oxidation of Rh(III) to Rh(IV) is needed which enables the reductive elimination via **XIV-TS** with a computed barrier of 17.6 kcal/mol. Intermediate **XIII** can easily undergo an one-electron oxidation to form the Rh(III) intermediate **XIV**, which releases product **4** via ligand exchange steps.

Scheme 2. Proposed catalytic mechanism of the rhodium catalyzed allylic acetylation going through Rh(IV)→Rh(II)

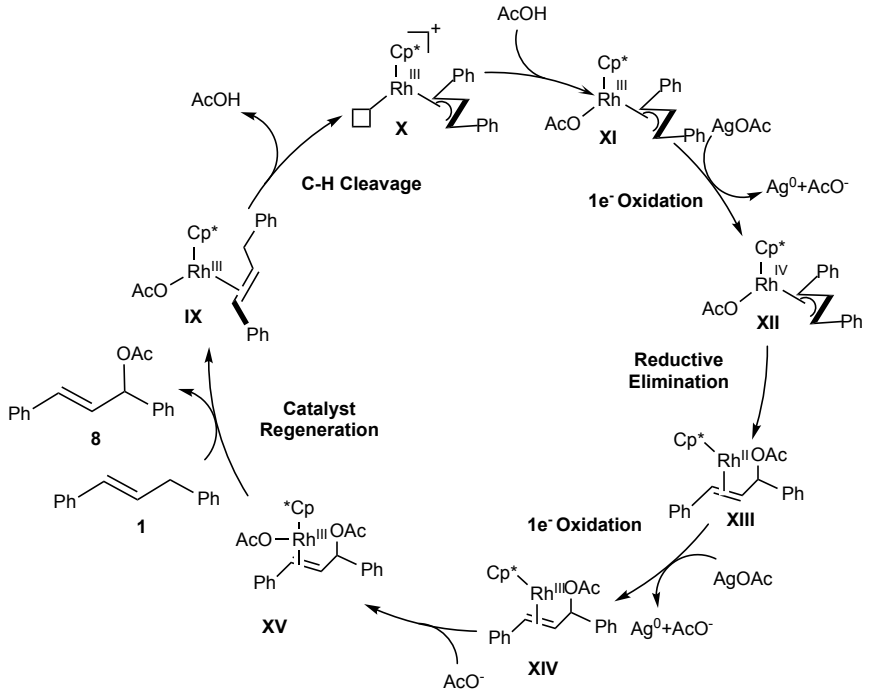

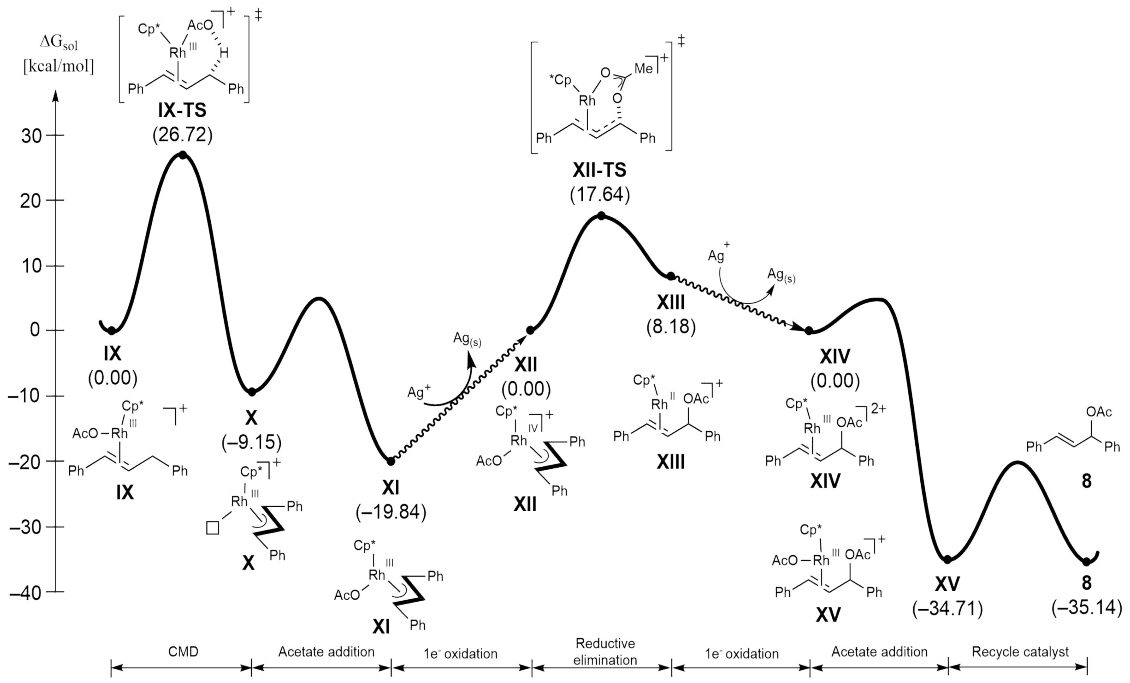

Figure 8. Energy profile for Rh-catalyzed allylic acetylation going through Rh (IV→II)

Formation of Allylic Amines With the detailed mechanism of the intermediate allylic acetate formation in hand, we turned our attention to the role of the silver and rhodium salts in the conversion of the allylic acetate to the allylic amine product, seeking to differentiate between simple Lewis acid promoted nucleophilic substitution or a more complicated allylic substitution proceeding through additional π-allyl complexes. In the following, we delineate the mechanistic details of the two possible mechanistic hypotheses for the formation of allylic amine product from the allylic acetate intermediate**,** by means of DFT calculations.

Scheme 3. Proposed mechanism for $AgSbF_6$ catalyzed allylic C–H amination from allylic acetate

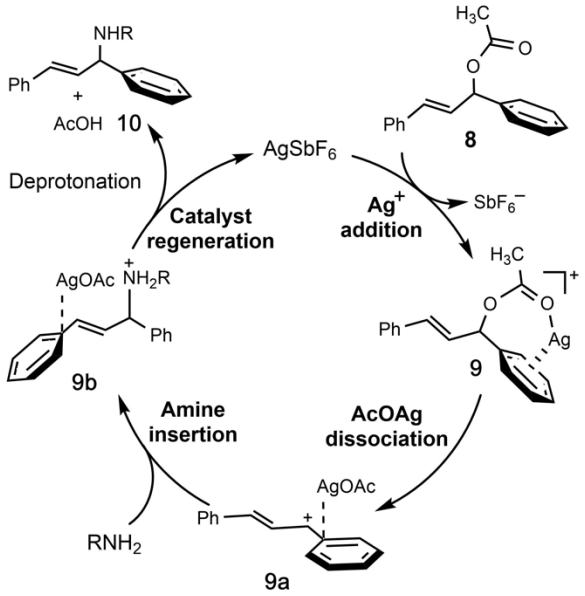

Inspired by the related $AgSbF_6$ catalyzed amination of allylic acetate,[12] we compiled a plausible mechanistic pathway for the amination reaction which involves an initial Ag^+ addition to allylic acetate to prepare a silver coordinated allylic acetate complex, as illustrated in Scheme 3. The energy profile for the allylic amination of allylic acetate **8** catalyzed by Ag^+ is depicted in Figure 9. The catalytic cycle is initiated by the addition of Ag^+ to allylic acetate intermediate yielding **9**. Out of the three possible scenarios of the nucleophilic substitutions (S_N1, S_n2, and S_N2'), our DFT calculations suggested that the S_N1 mechanism is the most plausible route for the nucleophilic substitution. The dissociation of AgOAc, facilitated by Ag^+ as a Lewis acid, yields an allylic cation intermediate **9a**, associated with an activation barrier of 14.4 kcal/mol (**9-TS**). The addition of nucleophile (**9a-TS**) requires 16.7 kcal/mol of activation energy, which is predicted to be the most difficult step to activate of the amination reaction, yet is viable under the reaction condition used. In comparison, the S_N2 and S_N2' reactions are much more difficult to activate with the calculated activation barriers being 23.0 and 27.6 kcal/mol, respectively. To push the reaction forward, the aminated intermediate **9b** undergoes a concerted deprotonation via traversing the transition structure **9b-TS** to produce the allylic amine product bound to a silver cation **9c**.

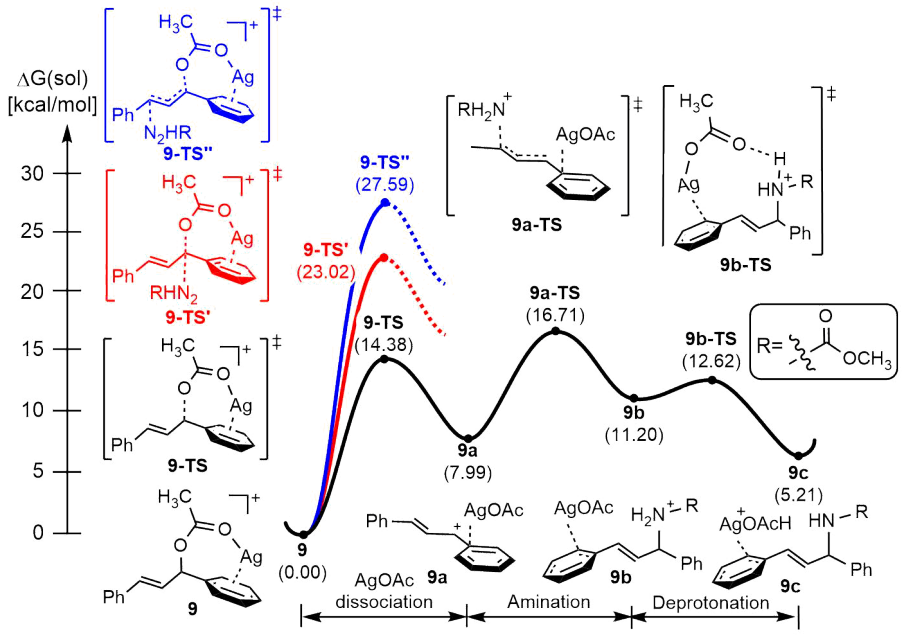

Figure 9. Energy profile for $AgSbF_6$ catalyzed allylic C–H amination from allylic acetate

Scheme 4. Proposed mechanism of the inner-sphere Rh-catalyzed allylic C–H amination from allylic acetate

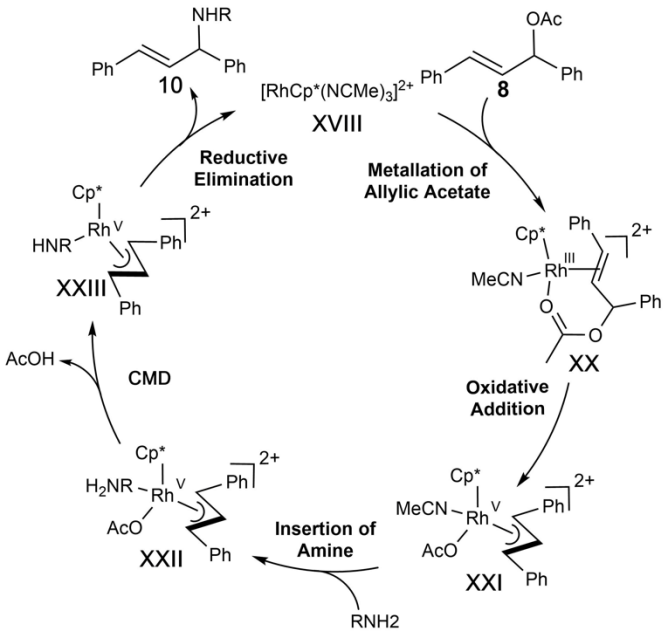

The catalytic cycle for a Cp*Rh catalyzed allylic amination of allylic acetate via the inner–sphere mechanism is depicted schematically in Scheme 4. A complete energy profile of the inner-sphere amination is depicted in Figure 10. To reduce the computational cost, we simplified the amine source to methylcarbamate. Commencing from the active catalyst **XVIII**, an intermediate **XIX** is formed through coordination of the allylic double bond, that is 12.8 kcal/mol uphill in energy. A ligand exchange step follows to allow the acetate of the substrate to coordinate the metal center to form **XX**, that is found at 9.5 kcal/mol higher in energy from that of the active catalyst. Subsequent oxidative addition of acetate takes places to yield an intermediate **XXI** that is 15.9 kcal/mol uphill in energy, via traversing the transition state **XX–TS** with an activation barrier of 22.8 kcal/mol. After the addition of acetate, a ligand exchange step follows to replace a coordinating acetonitrile with the amine ligand (**XXII**). The amine ligand undergoes a concerted metalation and deprotonation step (CMD) with the removal of an acetic acid molecule via a transition structure (**XXII–TS**) with the activation barrier of 26.2 kcal/mol, to find an intermediate **XXIII** that is 20.1 kcal/mol uphill in energy. In the next step, Rh(V) complex undergoes the reductive elimination from Rh(V)→Rh(III) to construct a new C–N bond via traversing a transition structure **XXIII–TS** with an activation energy barrier of 27.3 kcal/mol. The reductive elimination is the most difficult step to activate throughout the inner-sphere amination pathway. The computed activation energy barrier is moderately high yet is predicted to be viable under the reaction conditions used in some of the catalytic amination reactions (60°C), as the computed Eyring rate of the activation is 0.2 mol/day at 60°C. Upon completion of the reductive elimination, ligand exchanges steps follow to yield the aminated product **10** and to regenerate the catalyst **XXIII**. We also investigated the nucleophilic substitution of acetate by amine via the outer-sphere mechanism (Scheme S4 and Figure S10), and found a computed activation energy barrier for the amination of 41.0 kcal/mol, precluding this mechanism under the reaction conditions used.

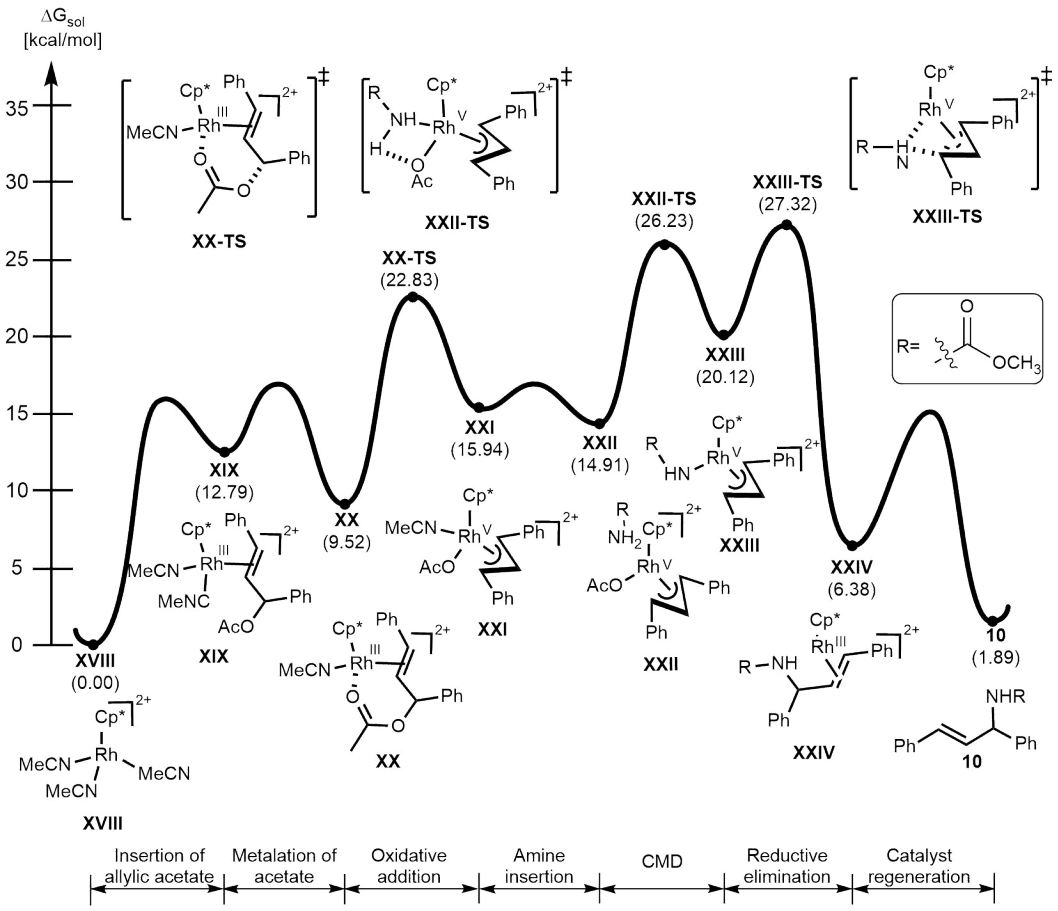

Figure 10. energy profile of the inner-sphere Rh-catalyzed amination of allylic acetate **4**

CONCLUSIONS

The computational and experimental data provided a detailed picture of the rhodium-catalyzed C(sp^3)–H allylic amination. Overall, the rate-determining step of the entire catalytic cycles examined computationally was found to be the C–H activation of allylic substrate with a DFT-computed barrier of 26.8 kcal/mol. This is consistent with the experimental kinetic observations that also support C–H activation as the rate determining step in this transformation. Calculations revealed that the Rh catalyst facilitates the formation of the allylic acetate using the silver salt as an oxidizing agent via an oxidatively induced reductive elimination reaction[11] where the Rh(III) center of the key intermediate is first oxidized to Rh(IV). Interestingly, the two-electron oxidation to possibly access the Rh(V) analogue is not found to be helpful and we found good experimental evidence that Rh(IV) is indeed the catalytically competent species. Further experimental studies as well as DFT calculations suggested that the amination of the allylic acetate intermediate proceeds by an S_N1 ligand exchange mechanism mediated by silver acting as a Lewis acid catalyst. Although a Cp*Rh catalyzed pathway was calculated to be feasible under the reaction conditions, the barriers were significantly higher than those calculated for the silver promoted pathway, and are unlikely to contribute significantly to product formation. We note that this study provides insights that are likely applicable to the related rhodium catalyzed allylic etherification and arylation reactions that were recently disclosed,[13] but likely do not explain the allylic arylation reaction utilizing aryl boronic acids,[14] or the allylic amidation

processes using dioxazolone reagents.[15] Further studies to provide a unified mechanistic picture of this emergent field are required.

Computational details

All calculations were constructed using computer models based on density functional theory (DFT)[16] implemented in the Jaguar 9.1 suite[17] of ab initio quantum chemistry programs. Geometry optimizations were performed using the B3LYP[18] functional including Grimme's D3 dispersion correction[19] and the 6-31G(d,p) basis set, where rhodium was represented with the Los Alamos LACVP basis set,[20] which incorporates effective core potentials that describes the relativistic effects (B3LYP-D3/LACVP). Upon completion of the geometry optimizations, single point SCF electronic energies of the optimized geometries were calculated using Dunning's correlation consistent triple-ζ basis set (cc-pVTZ(-f))[21] that includes a double set of the polarization functions. For rhodium, a modified version of LACVP, designed as LACV3P is used to match the effective core potential with triple-ζ quality was used for the single point SCF calculations (B3LYP-D3/cc-pVTZ(–f)/LACV3P). Solvation energies were evaluated using the self-consistent reaction field (SCRF)[22] approach based on the accurate numerical solutions of the Poisson-Boltzmann equation. For the solvation calculations, 6-31G(d,p)/LACVP basis at the optimized gas-phase geometries were used with the solvent dielectric constant of ε = 9.08 for the solvent medium considered (1,2-dichloroethane). It is noted that the solvation energies are contingent on the empirical parameterization of atomic radii used to generate the solute surface, wherein we used the standard set of optimized radii for H (1.150 Å), C (1.900 Å), N (1.600 Å), O (1.550 Å), Ag (1.574 Å), Sb (2.210 Å), F (1.682 Å), and Rh (1.464 Å) that are employed in the Jaguar 9.1 suite.[23] To confirm the proper convergence to well-defined minima (intermediates and products) or saddle points (transition structures) on the potential energy surface, vibrational frequencies based on harmonic approximation were computed with the 6-31G**/LACVP basis set. The energy components were calculated by adopting the protocol given below (eqs 2–6):

$$G(Sol) = G(gas) + G(solv) \quad (2)$$

$$G(gas) = H(gas) - TS(gas) \quad (3)$$

$$H(gas) = E(SCF) + ZPE \quad (4)$$

$$\Delta E(SCF) = \Sigma E(SCF) \text{ for products} - \Sigma E(SCF) \text{ for reactants} \quad (5)$$

$$\Delta G(sol) = \Sigma G(sol) \text{ for products} - \Sigma G(sol) \text{ for reactants} \quad (6)$$

, G(sol) is the Gibbs free energy in solution phase, G(gas) is the Gibbs free energy in gas phase, G(solv) is the free energy of solvation, H(gas) is the enthalpy in gas phase, T is the temperature (298.15 K), S(gas) is the entropy in gas phase, ZPE is the zero point energy, and E(SCF) is the self-consistent electronic field energy calculated by the SCF procedure.[24]

ASSOCIATED CONTENT

Supporting Information

The supporting Information is available free of charge on the ACS Publications website at DOI:

Author Information

Corresponding Author

*E-mail: mbaik2805@kaist.ac.kr

*E-mail: sblakey@emory.edu

ORCID

Mu-Hyun Baik: 0000-0002-8832-8187

Simon B. Blakey: 0000-0002-4100-8610

Jiyong Park: 0000-0002-3225-4510

Cora E. MacBeth: 0000-0003-3877-2236

Jaohn Bacsa: 0000-0001-5681-4458

Notes

The authors declare no competing financial interest.

ACKNOWLEDGMENT

The research was supported in part by the Institute for Basic Science (IBS-R010-DI) in Korea and by the National Science Foundation (NSF) under the CCI Center for Selective C-H Functionalization (CHE-1700982). NMR studies for this research were performed on instrumentation funded by the NSF (CHE-1531620). The X-ray analysis was done by the Emory X-ray Crystallography Facility using the Rigaku Synergy-S diffractometer, supported by the NSF (CHE-1626172).

REFERENCES

1. (a) Wang, N.-X.; Xing, Y.; Zhang, W., Advances in Transition-Metal-Catalyzed Direct sp3-Carbon–Hydrogen Bond Functionalization. *Synlett* **2015,** *26* (15), 2088-2098.(b) Yang, X.; Shan, G.; Wang, L.; Rao, Y., Recent advances in transition metal (Pd, Ni)-catalyzed C(sp 3) H bond activation with bidentate directing groups. *Tetrahedron Lett.* **2016,** *57* (8), 819-836.(c) Saint-Denis, T. G.; Zhu, R.-Y.; Chen, G.; Wu, Q.-F.; Yu, J.-Q., Enantioselective C(sp)–H bond activation by chiral transition metal catalysts. *Science* **2018,** *359* (6377).(d) Chu, J. C. K.; Rovis, T., Complementary Strategies for Directed C(sp)-H Functionalization: A Comparison of Transition-Metal-Catalyzed Activation, Hydrogen Atom Transfer, and Carbene/Nitrene Transfer. *Angew. Chem. Int. Ed Engl.* **2018,** *57* (1), 62-101.
2. Li, C.-J., Cross-Dehydrogenative Coupling (CDC): Exploring C−C Bond Formations beyond Functional Group Transformations. *Acc. Chem. Res.* **2009,** *42* (2), 335-344.
3. Chen, M. S.; Whilte, M. C., A Sulfoxide-Promoted, Catalytic Method for the Regioselective Synthesis of Allylic Acetates from Monosubstituted Olefins via C−H Oxidation. *J. Am. Chem. Soc.* **2004,** *126* (5), 1346-1347.
4. (a) Young, A. J.; White, M. C., Catalytic Intermolecular Allylic C-H Alkylation. *J. Am. Chem. Soc.* **2008,** *130* (43), 14090-14091.(b) Reed, S. A.; White, M. C., Catalytic Intermolecular Linear Allylic C−H Amination via Heterobimetallic Catalysis. *J. Am. Chem. Soc.* **2008,** *130* (11), 3316-3318.(c) Reed, S. A.; Mazzotti, A. R.; White,

M. C., A Catalytic, Brønsted Base Strategy for Intermolecular Allylic C−H Amination. *J. Am. Chem. Soc.* **2009,** *131* (33), 11701-11706.(d) Pattillo, C. C.; Strambeanu, I. I.; Calleja, P.; Vermeulen, N. A.; Mizuno, T.; White, M. C., Aerobic Linear Allylic C–H Amination: Overcoming Benzoquinone Inhibition. *J. Am. Chem. Soc.* **2016,** *138* (4), 1265-1272.(e) Ma, R.; White, M. C., C-H to C-N Cross-Coupling of Sulfonamides with Olefins. *J. Am. Chem. Soc.* **2018,** *140* (9), 3202-3205.(f) Fraunhoffer, K. J.; White, M. C., syn-1,2-Amino Alcohols via Diastereoselective Allylic C−H Amination. *J. Am. Chem. Soc.* **2007,** *129* (23), 7274-7276.(g) Chen, M. S.; Prabagaran, N.; Labenz, N. A.; White, M. C., Serial Ligand Catalysis: A Highly Selective Allylic C−H Oxidation. *J. Am. Chem. Soc.* **2005,** *127* (19), 6970-6971.(h) Campbell, A. N.; White, P. B.; Guzei, I. A.; Stahl, S. S., Allylic C−H Acetoxylation with a 4,5-Diazafluorenone-Ligated Palladium Catalyst: A Ligand-Based Strategy To Achieve Aerobic Catalytic Turnover. *J. Am. Chem. Soc.* **2010,** *132* (43), 15116-15119.

5. Cochet, T.; Bellosta, V.; Roche, D.; Ortholand, J.-Y.; Greiner, A.; Cossy, J., Rhodium(iii)-catalyzed allylic C–H bond amination. Synthesis of cyclic amines from ω-unsaturated N-sulfonylamines. *Chem. Commun.* **2012,** *48* (87), 10745.

6. Burman, J. S.; Blakey, S. B., Regioselective Intermolecular Allylic C−H Amination of Disubstituted Olefins via Rhodium/π-Allyl Intermediates. *Angew. Chem. Int. Ed Engl.* **2017,** *129* (44), 13854-13857.

7. (a) Leahy, D. K.; Evans, P. A., Rhodium(I)-Catalyzed Allylic Substitution Reactions and Their Applications to Target Directed Synthesis. *ChemInform* **2005,** *36* (33).(b) Evans, P. A.; Nelson, J. D., Conservation of Absolute Configuration in the Acyclic Rhodium-Catalyzed Allylic Alkylation Reaction: Evidence for an Enyl(σ–π) Organorhodium Intermediate. *J. Am. Chem. Soc.* **1998,** *120* (22), 5581-5582.

8. (a) Satoh, T.; Miura, M., Oxidative coupling of aromatic substrates with alkynes and alkenes under rhodium catalysis. *Chemistry* **2010,** *16* (37), 11212-11222.(b) *Issues in Chemistry and General Chemical Research: 2011 Edition*. ScholarlyEditions: 2012; p 6580.

9. (a) Vásquez-Céspedes, S.; Wang, X.; Glorius, F., Plausible Rh(V) Intermediates in Catalytic C–H Activation Reactions. *ACS Catal.* **2017,** *8* (1), 242-257.(b) Li, L.; Brennessel, W. W.; Jones, W. D., An Efficient Low-Temperature Route to Polycyclic Isoquinoline Salt Synthesis via C−H Activation with $[Cp^*MCl_2]_2$(M = Rh, Ir). *J. Am. Chem. Soc.* **2008,** *130* (37), 12414-12419.

10. (a) Periana, R. A.; Bergman, R. G., Rapid intramolecular rearrangement of a hydrido(cyclopropyl)rhodium complex to a rhodacyclobutane. Independent synthesis of the metallacycle by addition of hydride to the central carbon atom of a cationic rhodium π-allyl complex. *J. Am. Chem. Soc.* **1984,** *106* (23), 7272-7273.(b) Wakefield, J. B.; Stryker, J. M., Metallacyclobutanes from kinetic nucleophilic addition to η^3-allyl ethylene complexes of iridium. Regioselectivity dependence on nucleophile and allyl orientation. *J. Am. Chem. Soc.* **1991,** *113* (18), 7057-7059.(c) Shibata, Y.; Kudo, E.; Sugiyama, H.; Uekusa, H.; Tanaka, K., Facile Generation and Isolation of π-Allyl Complexes from Aliphatic Alkenes and an Electron-Deficient Rh(III) Complex: Key Intermediates of Allylic C–H Functionalization. *Organometallics* **2016,** *35* (10), 1547-1552.

11. Shin, K.; Park, Y.; Baik, M.-H.; Chang, S., Iridium-catalysed arylation of C–H bonds enabled by oxidatively induced reductive elimination. *Nat. Chem.* **2017,** *10*, 218.

12. Dagar, A.; Guin, S.; Samanta, S., AgSbF6 -Catalyzed Tandem Reaction of 2-Alkynylanilines with Cyclic Enynones: Efficient access to 3-Furo[3,2-c]chromenylindoles and Related Scaffolds. *Asian J. Org. Chem.* **2017,** *7* (1), 123-127.

13. (a) Nelson, T. A. F.; Blakey, S. B., Intermolecular Allylic C−H Etherification of Internal Olefins. *Angew. Chem. Int. Ed Engl.* **2018,** *130* (45), 15127-15131.(b) Lerchen, A.; Knecht, T.; Koy, M.; Ernst, J. B.; Bergander, K.; Daniliuc, C. G.; Glorius, F., Non-Directed Cross-Dehydrogenative (Hetero) arylation of Allylic C (sp3)- H bonds enabled by C- H Activation. *Angew. Chem. Int. Ed.* **2018,** *57* (46), 15248-15252.

14. Knecht, T.; Pinkert, T.; Dalton, T.; Lerchen, A.; Glorius, F., Cp^*Rh^{III}-Catalyzed Allyl–Aryl Coupling of Olefins and Arylboron Reagents Enabled by C(sp3)–H Activation. *ACS Catal.* **2019,** *9* (2), 1253-1257.

15. (a) Lei, H.; Rovis, T., Ir-Catalyzed Intermolecular Branch-Selective Allylic C-H Amidation of Unactivated Terminal Olefins. *J. Am. Chem. Soc.* **2019,** *141* (6), 2268-2273.(b) Knecht, T.; Mondal, S.; Ye, J.-H.; Das, M.; Glorius, F., Intermolecular, Branch-Selective, and Redox-Neutral Cp^*Ir^{III} -Catalyzed Allylic C−H Amidation. *Angew. Chem. Int. Ed Engl.* **2019,** *58* (21), 7117-7121.(c) Burman, J. S.; Harris, R. J.; B. Farr, C. M.; Bacsa, J.; Blakey, S. B., Rh(III) and Ir(III)Cp* Complexes Provide Complementary Regioselectivity Profiles in Intermolecular Allylic C–H Amidation Reactions. *ACS Catal.* **2019**, 5474-5479.

16. Parr, R. G.; Yang, W., *Density-Functional Theory of Atoms and Molecules*. Oxford University Press: 1994.

17. Bochevarov, A. D.; Harder, E.; Hughes, T. F.; Greenwood, J. R.; Braden, D. A.; Philipp, D. M.; Rinaldo, D.; Halls, M. D.; Zhang, J.; Friesner, R. A., Jaguar: A high-performance quantum chemistry software program with strengths in life and materials sciences. *Int. J. Quantum Chem.* **2013,** *113* (18), 2110-2142.

18. (a) Becke, A. D., Density-Functional Theromochemistry 3. The Role of Exact Exchange. *J. Chem. Phys.* **1993,** *98* (7), 5648-5652.(b) Lee, C.; Yang, W.; Parr, R. G., Development of the Colle-Salvetti correlation-energy formula into a functional of the electron-density. *Phys. Rev. B* **1988,** *37* (2), 785-789.

19. Grimme, S.; Antony, J.; Ehrlich, S.; Krieg, H., A consistent and accurate ab initio parametrization of density functional dispersion correction (DFT-D) for the 94 elements H-Pu. *J. Chem. Phys.* **2010,** *132* (15).
20. (a) Hay, P. J.; Jeffrey Hay, P.; Wadt, W. R., Ab initio effective core potentials for molecular calculations. Potentials for K to Au including the outermost core orbitals. *J. Chem. Phys.* **1985,** *82* (1), 299-310.(b) Wadt, W. R.; Jeffrey Hay, P., Ab initio effective core potentials for molecular calculations. Potentials for main group elements Na to Bi. *J. Chem. Phys.* **1985,** *82* (1), 284-298.(c) Hay, P. J.; Jeffrey Hay, P.; Wadt, W. R., Ab initio effective core potentials for molecular calculations. Potentials for the transition metal atoms Sc to Hg. *J. Chem. Phys.* **1985,** *82* (1), 270-283.
21. Dunning, T. H., Gaussian basis sets for use in correlated molecular calculations. I. The atoms boron through neon and hydrogen. *J. Chem. Phys.* **1989,** *90* (2), 1007-1023.
22. (a) Friedrichs, M.; Zhou, R.; Edinger, S. R.; Friesner, R. A., Poisson−Boltzmann Analytical Gradients for Molecular Modeling Calculations. *J. Phys. Chem. B* **1999,** *103* (16), 3057-3061.(b) Marten, B.; Kim, K.; Cortis, C.; Friesner, R. A.; Murphy, R. B.; Ringnalda, M. N.; Sitkoff, D.; Honig, B., New Model for Calculation of Solvation Free Energies: Correction of Self-Consistent Reaction Field Continuum Dielectric Theory for Short-Range Hydrogen-Bonding Effects. *J. Phys. Chem.* **1996,** *100* (28), 11775-11788.(c) Edinger, S. R.; Cortis, C.; Shenkin, P. S.; Friesner, R. A., Solvation Free Energies of Peptides: Comparison of Approximate Continuum Solvation Models with Accurate Solution of the Poisson−Boltzmann Equation. *J. Phys. Chem. B* **1997,** *101* (7), 1190-1197.
23. Rashin, A. A.; Honig, B., Reevaluation of the Born model of ion hydration. *J. Phys. Chem.* **1985,** *89* (26), 5588-5593.
24. Ryu, H.; Park, J.; Kim, H. K.; Park, J. Y.; Kim, S.-T.; Baik, M.-H., Pitfalls in Computational Modeling of Chemical Reactions and How To Avoid Them. *Organometallics* **2018,** *37* (19), 3228-3239.